LINEAR AND NONLINEAR VIBRATIONS OF SHELLS

Francesco Pellicano

Dipartimento di Ingegneria Meccanica e Civile, Università di Modena e Reggio Emilia, V.Vignolese, 905 41100 Modena Italy, Tel. +39 059 2056154, Fax. +39 059 2056129, e-mail: francesco.pellicano@unimore.it

Keywords: shells, vibration, chebyshev polynomials.

Abstract. *In the present paper linear and nonlinear vibrations of circular cylindrical shells having different boundary conditions are analyzed by means of the Sanders-Koiter theory. Displacement fields are expanded in a mixed double series based on harmonic functions and Chebyshev polynomials.*

Simply supported and clamped-clamped boundary conditions are analyzed, as well as connection with rigid bodies; in the latter case experiments are carried out. Comparisons with experiments and finite element analyses show that the technique is computationally efficient and accurate in modelling linear vibrations of shells with different boundary conditions.

An application to large amplitude of vibration shows that the technique is effective also in the case of nonlinear vibration: comparisons with the literature confirm the accuracy of the approach.

1. INTRODUCTION

The continuous growing of the commercial use of Space facilities lead to the development of new and more efficient aerospace vehicles; therefore, new and accurate studies on light-weight, thin-walled structures are needed. A wide part of the technical literature in the past century was focalized on the analysis of thin-walled structures and tried to investigate their behaviour in many different operating conditions, i.e. under static or dynamic loads, either in presence or absence of fluid-structure interaction. Both linear and nonlinear models have been developed to forecast the response of such structures. Many studies were concerned with cylindrical shells that constitute main parts of aircrafts, rockets, missiles and generally aerospace structures.

The literature about vibration of shells is extremely wide and the reader can refer to Leissa [1] or more recently to Amabili and Païdoussis [2] for a comprehensive review of models and results present in literature. In the following some studies, strictly related to the present paper, are described.

Liew et al. [3] analyzed linear vibrations of shallow conical shells using two-dimensional orthogonal polynomials and the Ritz procedure, for obtaining frequencies and modes of vibration: the approach was mesh-free, but able to handle complex geometries and boundary conditions.

Bhaskar and Dumir [4] analyzed the dynamics of rectangular orthotropic plates, resting on a nonlinear elastic foundation: they used a discretization approach based on polynomials and orthogonal point collocation method, obtained from zeros of Legendre polynomials. The nonlinear dynamics was analyzed by means of the averaging method and backbone curves were obtained.

Liew et al. [5] analyzed conical shells by means of a mesh free approach based on the Ritz method and a mixed Fourier and polynomial expansion. They considered both simply supported and clamped boundary conditions. The same authors used the same approach for analyzing laminated cylindrical panels [6].

Zhou et al. [7] developed an approach based on Chebyshev polynomials and Ritz method for evaluating natural frequencies of solid and hollow cylinders. Soldatos and Messina [8] used orthogonal polynomials for analyzing laminated circular cylinders.

Nayfeh and Arafat [9] analyzed nonlinear axisymmetric vibrations of spherical shells, by means of Legendre polynomials for spatial discretizations, and multiple scale method for the dynamic scenario.

A special comment deserves the work of Trotsenko and Trotsenko [10], who studied vibrations of circular cylindrical shells with attached rigid bodies, by means of an approach quite close to the present theory. In Ref.[10] the authors used a mixed expansion based on trigonometric functions and Legendre polynomials; they considered only linear vibrations. One of these authors published recently a paper on the same subject [11], in which results and theory present in Ref. [3] are reprinted (such work is reported for completeness).

In the present paper, linear and nonlinear vibrations of circular cylindrical shells are analyzed. Sanders-Koiter theory is considered for shell modelling; in this theory, the shell deformation is described in terms of three displacements fields (longitudinal, circumferential and radial). Displacement fields are expanded by means of a double mixed series: harmonic functions for the circumferential variable; Chebyshev polynomials for the longitudinal variable. Then Lagrange equations are considered to obtain an ordinary differential equation system, from potential and kinetic energies and the virtual work of external forces.

Simply supported and clamped-clamped configurations are analyzed in detail, both comparing the present theory with exact solutions (for simply supported shells only) and finite elements. Moreover, a shell, clamped at the base and connected to a rigid body, is analyzed experimentally, analytically (present theory) and using standard finite elements models. The experimental setup is described as well as the experimental analysis, which includes frequency, damping and mode shape identification.

Nonlinear vibrations, due to large amplitude of vibration, are analyzed in the case of simply supported shells; the present theory is compared with the literature.

2. EQUATIONS OF MOTION

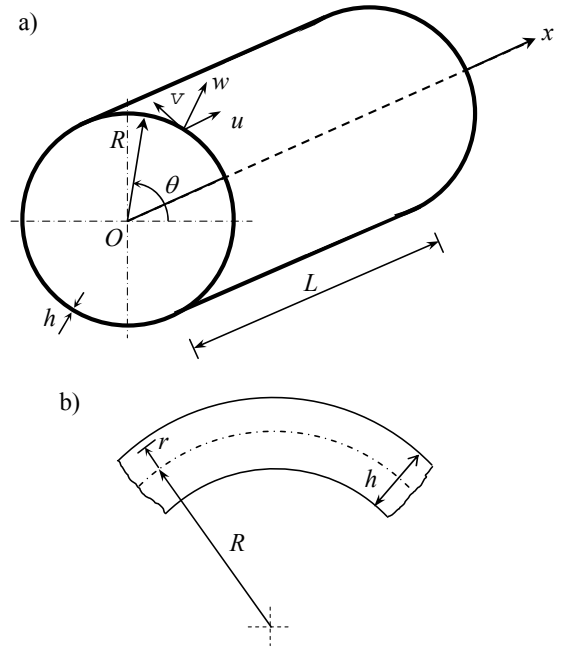

Figure 1. Circular cylindrical shell: coordinate system and dimensions. (a) Complete shell; (b) cross-section of the shell surface

In Figure 1 a circular cylindrical shell having radius R, length L and thickness h is represented; a cylindrical coordinate system ($O; x, r, \theta$) is considered in order to take advantage from the axial symmetry of the structure, the origin of the reference system is located at the centre of one end of the shell. In Figure 1 three displacement fields are represented: axial $u(x,\theta,t)$, circumferential $v(x,\theta,t)$ and radial $w(x,\theta,t)$.

Geometric imperfections can be considered in the theory by means of an initial radial displacement field $w_0(x,\theta)$; however, in the numerical results, only perfect shells are considered.

Strain Energy

The Sanders-Koiter theory is based on Love's first approximation: (i) $h<<R$; (ii) strains are small; (iii) transverse normal stresses are small; and (iv) the normal to the undeformed middle surface remains straight and normal to the middle surface after deformation, no thickness stretching is present (Kirchhoff-Love kinematic hypothesis) [1,2,12]; (v) rotary inertia and shear deformations are neglected.

Strain components ε_x, ε_θ and $\gamma_{x\theta}$ at an arbitrary point of the shell are [1]:

$$\varepsilon_x = \varepsilon_{x,0} + r\,k_x, \qquad \varepsilon_\theta = \varepsilon_{\theta,0} + r\,k_\theta \quad \gamma_{x\theta} = \gamma_{x\theta,0} + r\,k_{x\theta} \tag{1}$$

where: $\varepsilon_{x,0}$, $\varepsilon_{\theta,0}$ and $\gamma_{x\theta,0}$ are middle surface strains; k_x, k_θ and $k_{x\theta}$ are curvature and torsion changes of the middle surface; and r is the distance of the arbitrary point of the shell from the middle surface (see Figure 1(b)).

According to the Sanders-Koiter theory, middle surface strains and changes in the curvature and torsion are given by [1,2]:

$$\varepsilon_{x,0} = \frac{\partial u}{L\partial\eta} + \frac{1}{2}\left(\frac{\partial w}{L\partial\eta}\right)^2 + \frac{1}{8}\left(\frac{\partial v}{L\partial\eta} - \frac{\partial u}{R\partial\theta}\right)^2 + \frac{\partial w}{L\partial\eta}\frac{\partial w_0}{L\partial\eta} \tag{2a}$$

$$\varepsilon_{\theta,0} = \frac{\partial v}{R\partial\theta} + \frac{w}{R} + \frac{1}{2}\left(\frac{\partial w}{R\partial\theta} - \frac{v}{R}\right)^2 + \frac{1}{8}\left(\frac{\partial u}{R\partial\theta} - \frac{\partial v}{L\partial\eta}\right)^2 + \frac{\partial w_0}{R\partial\theta}\left(\frac{\partial w}{R\partial\theta} - \frac{v}{R}\right), \tag{2b}$$

$$\gamma_{x\theta,0} = \frac{\partial u}{R\partial\theta} + \frac{\partial v}{L\partial\eta} + \frac{\partial w}{L\partial\eta}\left(\frac{\partial w}{R\partial\theta} - \frac{v}{R}\right) + \frac{\partial w_0}{L\partial\eta}\left(\frac{\partial w}{R\partial\theta} - \frac{v}{R}\right) + \frac{\partial w}{L\partial\eta}\frac{\partial w_0}{R\partial\theta}, \tag{2c}$$

$$k_x = -\frac{\partial^2 w}{L^2\partial\eta^2}, \tag{2d}$$

$$k_\theta = \frac{\partial v}{R^2\partial\theta} - \frac{\partial^2 w}{R^2\partial\theta^2}, \tag{2e}$$

$$k_{x\theta} = -2\frac{\partial^2 w}{LR\partial\eta\partial\theta} + \frac{1}{2R}\left(3\frac{\partial v}{L\partial\eta} - \frac{\partial u}{R\partial\theta}\right) \tag{2f}$$

where $\eta=x/L$ is the nondimensional longitudinal coordinate.

The elastic strain energy U_S of a circular cylindrical shell, neglecting the radial stress σ_r (Love's first approximation), is given by [12]

$$U_S = \frac{1}{2} LR \int_0^{2\pi} \int_0^1 \int_{-h/2}^{h/2} \left(\sigma_x \varepsilon_x + \sigma_\theta \varepsilon_\theta + \tau_{x\theta} \gamma_{x\theta} \right) \mathrm{d}\eta \, (1 + r/R) \, \mathrm{d}\theta \, \mathrm{d}r , \tag{3}$$

In the case of homogeneous and isotropic materials, stresses σ_x, σ_θ and $\tau_{x\theta}$ are related to strains ($\sigma_r = 0$, case of plane stress) by [12]

$$\sigma_x = \frac{E}{1-\nu^2} \left(\varepsilon_x + \nu \varepsilon_\theta \right) , \qquad \sigma_\theta = \frac{E}{1-\nu^2} \left(\varepsilon_\theta + \nu \varepsilon_x \right) \qquad \tau_{x\theta} = \frac{E}{2(1+\nu)} \gamma_{x\theta} \tag{4}$$

where E is the Young's modulus and ν is the Poisson's ratio.

Using equations (1, 3, 4), the following expression of the potential energy is obtained

$$U_S = \frac{1}{2} \frac{Eh}{1-\nu^2} LR \int_0^{2\pi} \int_0^1 \left(\varepsilon_{x,0}^2 + \varepsilon_{\theta,0}^2 + 2\nu \varepsilon_{x,0} \varepsilon_{\theta,0} + \frac{1-\nu}{2} \gamma_{x\theta,0}^2 \right) \mathrm{d}\eta \, \mathrm{d}\theta + \frac{1}{2} \frac{Eh^3}{12(1-\nu^2)} LR \int_0^{2\pi} \int_0^1 \left(k_x^2 + k_\theta^2 + 2\nu k_x k_\theta + \frac{1-\nu}{2} k_{x\theta}^2 \right) \mathrm{d}\eta \, \mathrm{d}\theta + O(h^4) \tag{5}$$

where $O(h^4)$ is a higher-order term in h according to the Sanders-Koiter theory.

The first term of the right end side of equation (5) is the membrane energy (also referred to stretching) and the second one is the bending energy.

The kinetic energy T_S of a circular cylindrical shell (rotary inertia is neglected) is given by

$$T_S = \frac{1}{2} \rho_S \, h \, L \, R \int_0^{2\pi} \int_0^1 \left(\dot{u}^2 + \dot{v}^2 + \dot{w}^2 \right) \mathrm{d}\eta \, \mathrm{d}\theta , \tag{6}$$

where ρ_S is the mass density of the shell, the overdot denotes a time derivative.

The virtual work W done by the external forces is written as

$$W = LR \int_0^{2\pi} \int_0^1 \left(q_x u + q_\theta v + q_r w \right) \mathrm{d}\eta \, \mathrm{d}\theta , \tag{7}$$

where q_x, q_θ and q_r are the distributed forces per unit area acting in axial, circumferential and radial directions, respectively.

In-plane forces and bending moments depend on the shell strain; in the following, only relationships used in applying boundary conditions are reported:

$$M_x = \frac{Eh^3}{12(1-\nu^2)} \left(k_x + \nu k_\theta \right) , \qquad N_x = \frac{Eh}{1-\nu^2} \left(\varepsilon_{x,0} + \nu \varepsilon_{\theta,0} \right) \tag{8}$$

3. LINEAR VIBRATION: MODAL ANALYSIS.

In order to carry out a linear vibration analysis, in the present section linear Sanders-Koiter theory is considered, i.e. in equation (5), only quadratic terms are retained.

The best basis for expanding displacement fields is the eigenfunction basis; only for special boundary conditions such basis can be found analytically; generally, eigenfunctions must be evaluated in approximate way.

In order to attack the general problem of circular cylindrical shell vibration, displacement fields are expanded by means of a double series: the axial symmetry of the geometry and the periodicity of the deformation in the circumferential direction, leads to use harmonic functions; Chebyshev polynomials are considered in the axial direction.

Let us now consider a modal vibration, i.e. a synchronous motion:

$$u(\eta,\theta,t) = U(\eta,\theta) f(t) \qquad v(\eta,\theta,t) = V(\eta,\theta) f(t) \qquad w(\eta,\theta,t) = W(\eta,\theta) f(t) \tag{9}$$

where: $U(\eta,\theta)$, $V(\eta,\theta)$ and $W(\eta,\theta)$ represent the modal shape.

The modal shape is now expanded in a double series, in terms of Chebyshev polynomials $T_m^*(\eta)$, and harmonic functions:

$$U(\eta,\theta) = \sum_{m=0}^{M_U} \sum_{n=0}^{N} \tilde{U}_{m,n} T_m^*(\eta) \cos n\theta , \qquad V(\eta,\theta) = \sum_{m=0}^{M_V} \sum_{n=0}^{N} \tilde{V}_{m,n} T_m^*(\eta) \sin n\theta \qquad W(\eta,\theta) = \sum_{m=0}^{M_W} \sum_{n=0}^{N} \tilde{W}_{m,n} T_m^*(\eta) \cos n\theta \tag{10}$$

where $T_m^*(\eta) = T_m(2\eta - 1)$ and $T_m(\cdot)$ is the m-th order Chebyshev polynomial [13].

Note that, in absence of imperfections, a linear mode has the following simplified expression:

$$U(\eta,\theta) = \sum_{m=0}^{M_U} \tilde{U}_{m,n} T_m^*(\eta) \cos n\theta , \quad V(\eta,\theta) = \sum_{m=0}^{M_V} \tilde{V}_{m,n} T_m^*(\eta) \sin n\theta , \quad W(\eta,\theta) = \sum_{m=0}^{M_W} \tilde{W}_{m,n} T_m^*(\eta) \cos n\theta \tag{11}$$

Expansions (10) or (11) do not satisfy any particular boundary condition.

Boundary conditions

Some of the coefficients $\tilde{U}_{m,n}$, $\tilde{V}_{m,n}$ and $\tilde{W}_{m,n}$ of the equation (11) can be suitably chosen in order to satisfy boundary conditions.

Simply supported

The following boundary conditions are imposed to the mode shape:

$$w=0,\ v=0,\ M_x=0,\ N_x=0 \text{ for } \eta=0,1 \tag{12}$$

which imply

$$W(\eta,\theta)=\sum_{m=0}^{M_W}\sum_{n=0}^{N}\tilde{W}_{m,n}T_m^*(\eta)\cos n\theta=0, \qquad \text{for } \eta=0,1, \tag{13a}$$

$$V(\eta,\theta)=\sum_{m=0}^{M_V}\sum_{n=0}^{N}\tilde{V}_{m,n}T_m^*(\eta)\sin n\theta=0, \qquad \text{for } \eta=0,1, \tag{13b}$$

$$W_{,\eta\eta}(\eta,\theta)=\sum_{m=0}^{M_W}\sum_{n=0}^{N}\tilde{W}_{m,n}T_{m,\eta\eta}^*(\eta)\cos n\theta=0, \qquad \text{for } \eta=0,1, \tag{13c}$$

$$U_{,\eta}(\eta,\theta)=\sum_{m=0}^{M_U}\sum_{n=0}^{N}\tilde{U}_{m,n}T_{m,\eta}^*(\eta)\cos n\theta=0, \qquad \text{for } \eta=0,1. \tag{13d}$$

where $(\cdot)_{,\eta}=\partial(\cdot)/\partial\eta$ and $(\cdot)_{,\eta\eta}=\partial^2(\cdot)/\partial\eta^2$.

Such conditions are valid for any θ and n, therefore equations (13a-d) are modified as follows:

$$\sum_{m=0}^{M_W}\tilde{W}_{m,n}T_m^*(\eta)=0, \qquad n=0,1,\dots \text{, for } \eta=0,1 \tag{14a}$$

$$\sum_{m=0}^{M_V}\tilde{V}_{m,n}T_m^*(\eta)=0, \qquad n=0,1,\dots \text{, for } \eta=0,1 \tag{14b}$$

$$\sum_{m=0}^{M_W}\tilde{W}_{m,n}T_{m,\eta\eta}^*(\eta)=0, \qquad n=0,1,\dots \text{, for } \eta=0,1 \tag{14c}$$

$$\sum_{m=0}^{M_U}\tilde{U}_{m,n}T_{m,\eta}^*(\eta)=0, \qquad n=0,1,\dots \text{, for } \eta=0,1 \tag{14d}$$

The linear algebraic system of equations (14) is solved in terms of the coefficients: $\tilde{U}_{1,n}$, $\tilde{U}_{2,n}$, $\tilde{V}_{0,n}$, $\tilde{V}_{1,n}$, $\tilde{W}_{0,n}$, $\tilde{W}_{1,n}$, $\tilde{W}_{2,n}$, $\tilde{W}_{3,n}$, n=0,1,...; which can be obtained exactly in terms of the remaining unknown coefficients. In the present work the solution of system (14) is carried out by means of algebraic manipulation software.

Clamped-Clamped

The following boundary conditions are imposed to the mode shape:

$$w=0,\ w_{,\eta\eta}=0,\ v=0,\ u=0, \text{ for } \eta=0,1 \tag{15}$$

The procedure followed to respect boundary conditions is formally the same of simply supported boundary conditions; however, the resulting linear system is solved in terms of the following coefficients: $\tilde{U}_{0,n}$,$\tilde{U}_{1,n}$,$\tilde{V}_{0,n}$,$\tilde{V}_{1,n}$, $\tilde{W}_{0,n}$, $\tilde{W}_{1,n}$, $\tilde{W}_{2,n}$, $\tilde{W}_{3,n}$, n=0,1,...

Clamped-disk-on-the-top

In this case both theoretical, experimental and finite elements analyses are carried out; therefore, a particular system is considered, in Figure 2 the geometry of the system as well as the dimensions are represented.

The shell is clamped at the bottom to a rigid support; therefore, for η=0 the boundary conditions are the same of the clamped-clamped case, equation (15).

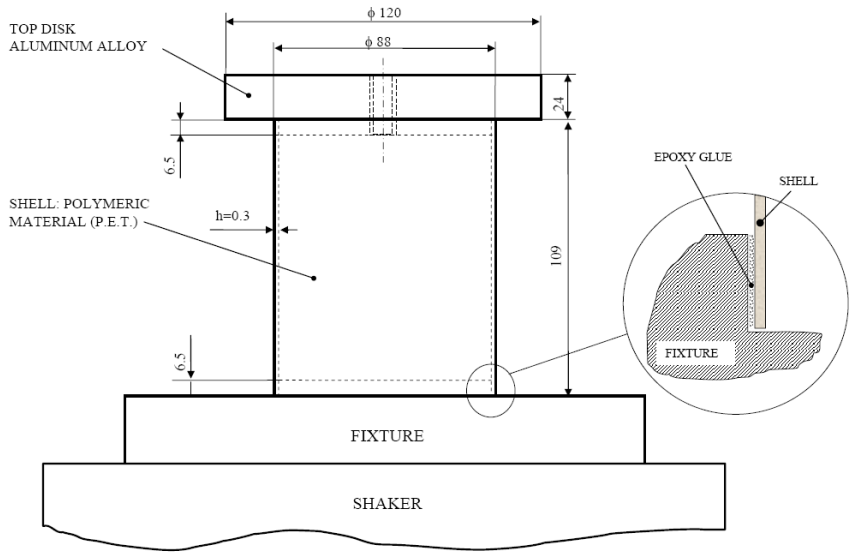

Figure 2. Configuration and dimensions (millimiters) of the system analyzed experimentally.

In order to impose boundary conditions to the top end of the shell, it is useful to consider the rigid body motion of the disk. Such a body has six degrees of freedom; however, in the present work torsional vibration is not considered; therefore, the number of degrees of freedom is reduced to five. Moreover, experiments evidenced that the rigid body motion presents extremely small amplitude; therefore, a linearized analysis of the disk motion will be performed in the following. Rigid body (disk) degrees of freedom are considered additional variables of the problem: in writing boundary conditions of the shell top-end, the rigid body motion is an imposed displacement.

Let us consider a Cartesian reference system (*O', x', y', z'*) having the origin located at the centre of the shell top-end (η=1), see Figure 4; note that, the origin of the circumferential coordinate θ (Figure 1) is set coincident with axis *y'* (Figure 4). S_{Dx}, S_{Dy}, S_{Dz} are three displacement components of the origin (*O'*) motion, see Figure 4. The rotation is treated in a simplified way: the small amplitude of the body motion allows to linearize the analysis and to apply the superposition principle; the global rotation is assumed to be a superposition of three rotations about three axes (*x',y',z'*).

Given an arbitrary and infinitesimal motion to the top-disk, Figure 4, and considering the shell clamped to the disk, one obtains the following boundary conditions:

$$u(L,\theta,t) = -R\alpha_y(t)\sin\theta - R\alpha_z(t)\cos\theta + S_{Dx}(t) \tag{16a}$$

$$v(L,\theta,t) = -S_{Dy}(t)\sin\theta - S_{Dz}(t)\cos\theta - R\alpha_x(t) \tag{16b}$$

$$w(L,\theta,t) = S_{Dy}(t)\cos\theta - S_{Dz}(t)\sin\theta \tag{16c}$$

$$\theta_\alpha = -\alpha_y(t)\sin\theta - \alpha_z(t)\cos\theta \tag{16d}$$

where $\theta_\alpha = -(1/L)(\partial w/\partial\eta)\big|_{x=L}$.

Note that equations (16) are in agreement with Ref. [10], where such conditions are obtained by means of a different approach.

It is to note that, for n>1 boundary conditions given by the rigid body motion correspond to clamping (see equations 14); moreover, axisymmetric modes (n=0) are influenced by S_{Dx} only.

Kinetic energy: disk on the top

The kinetic energy of the shell is given by equation (6); when a rigid body is connected to one of the shell ends, its kinetic energy must be added to the system.

A rigid body motion, imposed to the shell top end, induces a motion of the top-disk; in particular, the motion of its centre of mass *G* depends both on the displacement of *O'* and two rotations (see Figures 4 and 5). Assuming also infinitesimal rotations and linearizing all relationships, one easily obtains:

$$x_G(t) = S_{Dx}(t) \quad y_G(t) = S_{Dy}(t) + \alpha_z(t)h_G \qquad z_G(t) = S_{Dz}(t) - \alpha_y(t)h_G \tag{17}$$

If one is not interested in torsional vibrations of the shell, the rotation about *x'* axis can be neglected; therefore, the kinetic energy of the disk is given by:

$$T_D = \frac{1}{2}m_D\left(\dot{S}_{Dy} + \dot{\alpha}_z h_G\right)^2 + \frac{1}{2}m_D\left(\dot{S}_{Dz} - \dot{\alpha}_y h_G\right)^2 + \frac{1}{2}J_z\dot{\alpha}_z^2 + \frac{1}{2}J_y\dot{\alpha}_y^2 + \frac{1}{2}m_D\dot{S}_{Dx}^2 \tag{18}$$

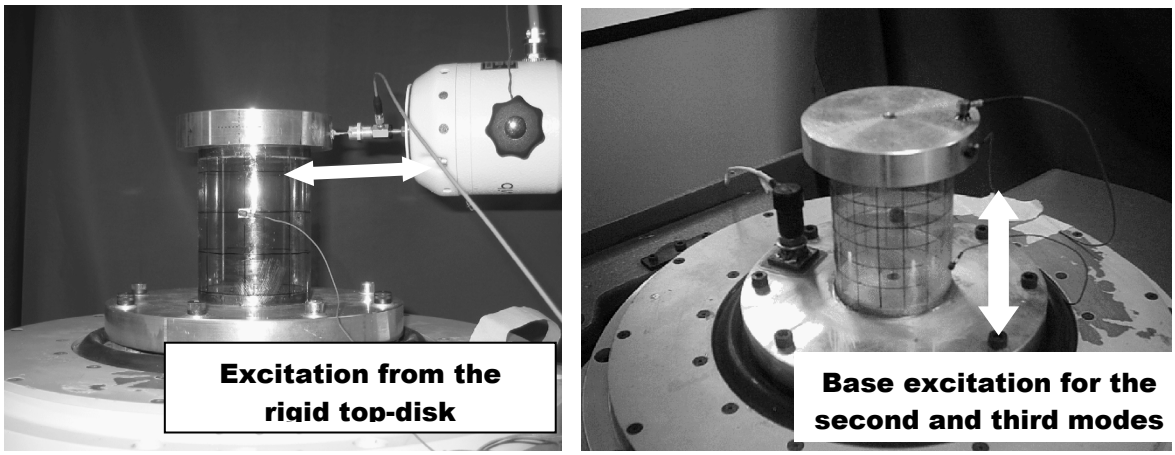

Figure 3. Experimental setup and excitation types.

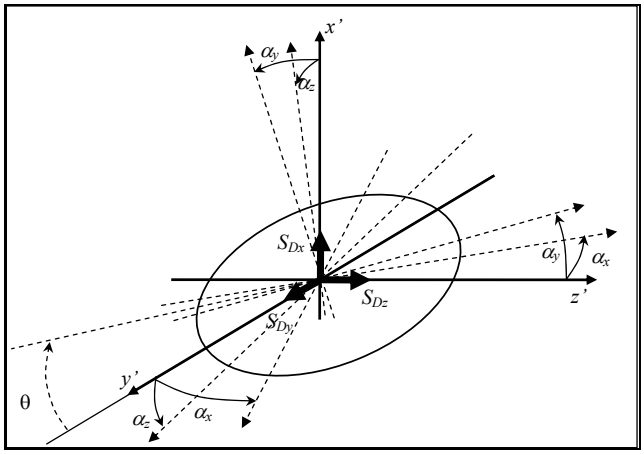

Figure 4. Rigid body motion imposed at the top shell end (η=1).

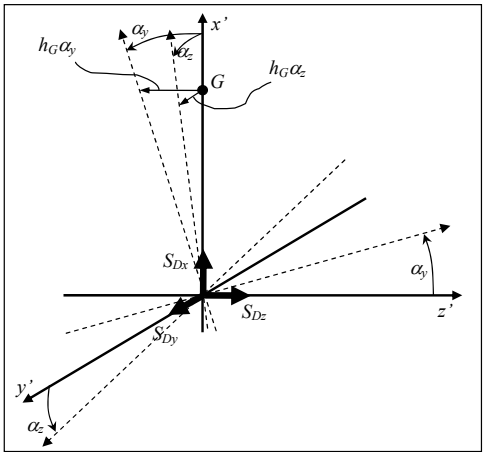

Figure 5. Displacement of the top disk centre of mass, due to a rigid body motion of the shell-top-end.

Discretization: Lagrange equations

Expansions (9) are introduced in the expressions of the kinetic and the potential energy (for the linear system); then a set of ordinary differential equations is obtained by using Lagrange equations.

An intermediate step is the reordering of variables, in order to proceed in a systematic way. A vector containing all variables is built depending on the boundary conditions.

Simply supported:

$$\mathbf{q}=\left[\tilde{U}_{0,0},\tilde{U}_{3,0},\tilde{U}_{4,0},...,\tilde{U}_{0,1},\tilde{U}_{3,1},\tilde{U}_{4,1},...,\tilde{V}_{2,0},\tilde{V}_{3,0},...,\tilde{V}_{2,1},\tilde{V}_{3,1},...,\tilde{W}_{4,0},\tilde{W}_{5,0},...,\tilde{W}_{4,1},\tilde{W}_{5,1},...,\right]f(t) \tag{19}$$

Clamped-clamped:

$$\mathbf{q}=\left[\tilde{U}_{2,0},\tilde{U}_{3,0},...,\tilde{U}_{2,1},\tilde{U}_{3,1},...,\tilde{V}_{2,0},\tilde{V}_{3,0},...,\tilde{V}_{2,1},\tilde{V}_{3,1},...,\tilde{W}_{4,0},\tilde{W}_{5,0},...,\tilde{W}_{4,1},\tilde{W}_{5,1},...,\right]f(t) \tag{20}$$

Rigid body connected to the shell:

$$\mathbf{q}=\left[\tilde{U}_{2,0},\tilde{U}_{3,0},...,\tilde{U}_{2,1},\tilde{U}_{3,1},...,\tilde{V}_{2,0},\tilde{V}_{3,0},...,\tilde{V}_{2,1},\tilde{V}_{3,1},...,\tilde{W}_{4,0},\tilde{W}_{5,0},...,\tilde{W}_{4,1},\tilde{W}_{5,1},...,\tilde{S}_{Dx},\tilde{S}_{Dy},\tilde{S}_{Dz},\tilde{\alpha}_y,\tilde{\alpha}_z\right]f(t) \tag{21}$$

where $S_{Dx}=f(t)\tilde{S}_{Dx}$, $S_{Dy}=f(t)\tilde{S}_{Dy}$, $S_{Dz}=f(t)\tilde{S}_{Dz}$, $\alpha_y=f(t)\tilde{\alpha}_y$, $\alpha_z=f(t)\tilde{\alpha}_z$.

Note that the torsional degree of freedom of the disk is neglected in the present paper; therefore, α_x is not included in equation (21). Moreover, a unique time law $f(t)$ is considered in order to impose a synchronous motion (modal vibration); such assumption will be relaxed in the case of nonlinear vibration.

The maximum number of variables needed for describing a generic mode with n nodal diameters is: $N_P=M_U+M_V+M_W-5$ without connected rigid body and $N_P=M_U+M_V+M_W$ with the rigid body.

Lagrange equations for free vibrations are:

$$\frac{d}{dt}\left(\frac{\partial L}{\partial \dot{q}_i}\right)-\frac{\partial L}{\partial q_i}=0 \quad i=1,2,\ldots N_{\max} \tag{22}$$

where $L=T-U_S$; $T=T_S+T_D$, $N_{max}=N_P*N$.

Using equation (19) and considering an harmonic motion, $f(t)=e^{j\omega t}$, one obtains:

$$\left(-\omega^2\mathbf{M}+\mathbf{K}\right)\mathbf{q}=\mathbf{0} \tag{23}$$

which is the classical non-standard eigenvalue problem that furnishes frequencies and modes of vibration

(eigenvalues and eigenvectors).

A modal shape corresponding to the *j*-th mode is given by:

$$U^{(j)}(\eta,\theta)=\sum_{m=0}^{M_U}\sum_{n=0}^{N}\tilde{U}_{m,n}^{(j)}T_m^*(\eta)\cos n\theta,\quad V^{(j)}(\eta,\theta)=\sum_{m=0}^{M_V}\sum_{n=0}^{N}\tilde{V}_{m,n}^{(j)}T_m^*(\eta)\sin n\theta\quad W^{(j)}(\eta,\theta)=\sum_{m=0}^{M_W}\sum_{n=0}^{N}\tilde{W}_{m,n}^{(j)}T_m^*(\eta)\cos n\theta \tag{24}$$

where $\tilde{U}_{m,n}^{(j)}$, $\tilde{V}_{m,n}^{(j)}$ and $\tilde{W}_{m,n}^{(j)}$ are components of the *j*-th eigenvector of equation (23) and the vector function $\left[U^{(j)}(x,\theta),V^{(j)}(x,\theta),W^{(j)}(x,\theta)\right]^T$ is the *j*-th eigenfunction of the original problem. Expansions (24) can be reduced to simple series in *m* when perfectly axial symmetric shells are considered.

A general motion can be expresses by expanding the displacement field using the modal basis:

$$u(x,\theta,t)=\sum_{j=1}^{N_{\max}}U^{(j)}(x,\theta)f_j(t)\qquad v(x,\theta,t)=\sum_{j=1}^{N_{\max}}V^{(j)}(x,\theta)f_j(t)\qquad w(x,\theta,t)=\sum_{j=1}^{N_{\max}}W^{(j)}(x,\theta)f_j(t) \tag{25}$$

where $f_i(t)$ is the modal coordinate.

Eigenfunctions are normalized by imposing that $\max\left[\max\left[U^{(j)}(x,\theta)\right],\max\left[V^{(j)}(x,\theta)\right],\max\left[W^{(j)}(x,\theta)\right]\right]=1$; the physical meaning of such normalization is the following: the modal coordinate $f_i(t)$ represents the maximum amplitude of vibration referred to the dominant direction of a mode shape (radial *w*, circumferential *v* or longitudinal *u*). For example, in the case of radial dominant modes, in the eigenfunction vector $\left[U^{(j)}(x,\theta),V^{(j)}(x,\theta),W^{(j)}(x,\theta)\right]^T$ the third component will have a maximum amplitude much larger than the others; if we normalize the vector function in order to have such maximum equal to 1, then $f_i(t)$ will give the maximum amplitude of vibration in the radial direction. The present normalization is particularly useful in nonlinear analyses.

4. NONLINEAR ANALYSIS

In the nonlinear analysis the full expression of potential shell energy (5), containing terms up to fourth order (cubic nonlinearity), is considered. Displacement fields $u(x,\theta,t)$, $v(x,\theta,t)$ and $w(x,\theta,t)$ are expanded by using linear mode shapes obtained in the previous section:

$$u(x,\theta,t)=\sum_{j=1}^{N_{\max}}U^{(j)}(x,\theta)f_{u,j}(t)\quad v(x,\theta,t)=\sum_{j=1}^{N_{\max}}V^{(j)}(x,\theta)f_{v,j}(t)\qquad w(x,\theta,t)=\sum_{j=1}^{N_{\max}}W^{(j)}(x,\theta)f_{w,j}(t) \tag{26}$$

Expansion (26a,b,c) respects boundary conditions, modal shapes $U^{(j)}(x,\theta)$, $V^{(j)}(x,\theta)$, $W^{(j)}(x,\theta)$, are known functions expressed in terms of polynomials and harmonic functions. It is to note that, in equations (26) the time function is different for each displacement field; therefore expansion (26) is an extension of expansion (25) and apparently it increases the number of degrees of freedom of the system. Conversely, using expansion (26) one can select suitable shapes for each displacement field separately, improving the convergence speed, reducing the number of degrees of freedom and increasing the computational accuracy.

Expansion (26) is put in the strain and kinetic energy (Eqs. (5), (6) or (15)) and in the virtual work expression (Eq. (7)) in the case of external excitation. Using Lagrange equations, a set of nonlinear ordinary differential equations is obtained; such system is then analyzed by using numerical continuation methods.

5. LINEAR ANALYSIS: NUMERICAL RESULTS

Numerical analyses are carried out on three test cases described below:

Case A (steel).

L = 0.2 m; R = 0.1m; h = 0.247×10^{-3}m; ρ = 2796kg/m^3; ν = 0.31; E = 71.02×10^{9}N/m^2.

Case B (aluminium alloy).

L = 0.2m; R = 0.2m; h = R/20; ρ= 7850 kg/m^3; ν=0.3; E = 2.1 10^{11}N/m^2;

Case C (P.E.T.+ disk on the top)

Shell: L=0.096m, R=0.044m, h=0.3×10^{-3}m, ρ= 1366 kg/m^3; ν=0.4.; E = 4.6 10^9 N/m^2;

Disk: m=0.82 kg, J_y=J_z=7.55×10^{-4} kg/m^2, h_G=0.01684 m.

Simply supported shells.

For such simple case eigenfunctions are known: $U(x,\theta)=u_{k,n,c}\cos n\theta\cos k\eta$; $V(x,\theta)=v_{k,n,c}\sin n\theta\sin k\eta$; $W(x,\theta)=w_{k,n,c}\cos n\theta\sin k\eta$, where n is the number of nodal diameters and k is the number of longitudinal half waves; eigenfrequencies can be easily computed by solving a polynomial equation; as well as ratios $w_{k,n,c}/u_{k,n,c}$ and $w_{k,n,c}/v_{k,n,c}$ [1].

Analyses are carried out on Case A, the first 34 modes are evaluated by means of exact theory, present method (polynomials of degree 9) and the commercial software MSC Marc (480×50 elements, 480 in the circumferential and 50 in the longitudinal directions, element type CQUAD4).

It is remarkable, that the shell exhibits a high modal density, 34 modes are within the frequency range (484.6-

1808Hz), see Table 1; such high modal density is typical for cylindrical shells. The difference between exact theory and the present approach is negligible (beyond the fourth digit). The finite element model gives accurate results, the error is less than 1%; however, this result has been obtained by means of a huge system having about 140 000 degrees of freedom; conversely, using the present approach, 22 dofs are needed, for obtaining one mode, when polynomials of degree 9 are used. Note that in Table 1 only four digits are used: this is the precision of MSC Marc output; therefore, for coherence, all results are reported with the same precision. Note that modes (k=3, n=10) and (k=2, n=6) are lost in the finite element analysis.

Mode		Natural frequencies [Hz]				
		Exact frequency	Present theory		FEM	
k	n		Freq.	Err. %	Freq.	Err. %
1	7	484.6	484.6	0	484.9	0.1
1	8	489.6	489.6	0	490.0	0.1
1	9	546.2	546.2	0	546.9	0.1
1	6	553.3	553.3	0	553.7	0.1
1	10	636.8	636.8	0	637.9	0.2
1	5	722.1	722.1	0	722.5	0.1
1	11	750.7	750.7	0	752.3	0.2
1	12	882.2	882.2	0	884.6	0.3
2	10	968.1	968.1	0	970.5	0.2
2	11	983.4	983.4	0	985.9	0.3
2	9	1018	1018	0	1021	0.3
1	13	1029	1029	0	1032	0.3
1	4	1041	1041	0	1042	0.1
2	12	1050	1050	0	1053	0.3
2	8	1148	1148	0	1150	0.2
2	13	1154	1154	0	1158	0.3
1	14	1189	1189	0	1194	0.4
2	14	1287	1287	0	1292	0.4
1	15	1362	1362	0	1368	0.4
2	7	1373	1373	0	1376	0.2
2	15	1443	1443	0	1449	0.4
3	12	1456	1456	0	1462	0.4
3	13	1470	1470	0	1477	0.5
3	11	1502	1502	0	1509	0.5
3	14	1536	1536	0	1543	0.5
1	16	1548	1548	0	1556	0.5
2	16	1617	1617	0	1626	0.6
3	10	1620	1620	0	-	-
1	3	1630	1630	0	1631	0.1
3	15	1643	1643	0	1651	0.5
2	6	1721	1721	0	-	-
1	17	1746	1746	0	1756	0.6
3	16	1782	1782	0	1792	0.6
2	17	1808	1808	0	1818	0.6

Table 1. Simply supported shell, case A. Comparison of natural frequencies: present theory vs. exact and finite elements results. Polynomials of degree 9 for the present theory.

Mode		Natural frequencies [Hz]		
		Exact frequency	Present theory	
k	n		Frequency	Error %
1	0	4140.74	4140.77	0.001
2	0	4788.34	4788.66	0.007
3	0	6890.30	6891.43	0.016
4	0	10655.3	10657.7	0.023
5	0	15900.6	15904.7	0.026
6	0	22497.1	22503.9	0.030
7	0	30384.4	30446.1	0.203
8	0	39533.9	39717.2	0.464
9	0	49930.3	48126.2	3.613
10	0	61563.5	64208.3	4.296

Table 2. Simply supported shell, case B. Comparison of axisymmetric modes natural frequencies: present theory vs. exact theory (only radial modes, w dominant). Polynomials of degree 15 for the present theory.

A second test is carried out on test case B, in order to check the accuracy of the polynomial expansion; in Table 2 the first 10 natural frequencies of axisymmetric modes are reported. In this case, polynomials used in the approximate method have degree equal to 15 (M_U=15, M_V=15, M_W=15, $N_P=M_U+M_V+M_W-5=40$). The accuracy is excellent up to the eighth mode, after such mode the number of longitudinal half waves (k=9, k=10 and so on)

cannot be approximated with great accuracy using polynomials of degree 15. However, also in the case of modes 9 and 10 the error is below 5%. In Table 2 only modes having a radially dominant vibration are considered, in order to check the convergence of the polynomial expansion; indeed, modes having a large number of longitudinal half waves are more difficult to simulate with polynomials.

For case B the fundamental mode is (k=1, n=4), the exact frequency is 2138,95 Hz; using polynomials of degree 5 (i.e. 10 dofs), we obtain 2139,19 Hz, the error is about 0.01%.

Clamped-clamped shells.

The Case A shell is considered for this analysis; simulations are carried out by using the present theory (polynomials of degree 7) and the finite element model having the same elements of the model described in the previous section. No exact analytical results are available for such case. Modes up to 1260 Hz are analyzed, i.e. the first 15 modes; in Table 3 natural frequencies are presented for comparison, k means that a mode has k-1 nodal circumferences (the meaning is similar to the simply supported case, even though the longitudinal displacement cannot be described by harmonic functions) and n is the number of nodal diameters. The agreement is excellent; indeed, the difference is less or equal to 1%. The number of degrees of freedom needed for describing a mode, using the present theory, is now 16.

Mode		Natural frequencies [Hz]		
		Finite elements	Present theory	Difference %
k	n			
1	9	685.4	687.7	0.3
1	8	697.3	701.7	0.6
1	10	727.2	727.9	0.1
1	7	775.2	782	0.9
1	11	809.7	809.2	0.1
1	12	922.2	920.5	0.2
1	6	930.1	939.6	1.0
1	13	1057	1055	0.2
2	11	1143	1144	0.1
2	10	1169	1172	0.3
2	12	1172	1172	0.0
1	5	1181	1193	1.0
1	14	1211	1207	0.3
2	13	1247	1245	0.2
2	9	1259	1264	0.4

Table 3. Clamped-clamped shell, case A. Comparison of natural frequencies: present theory vs. exact and finite elements results. Polynomials of degree 7 for the present theory.

6. EXPERIMENTAL AND THEORETICAL RESULTS: DISK ON THE TOP

The system under investigation is described in Figures 2 and 3. A circular cylindrical shell, made of a polymeric material (P.E.T., case C) is clamped at the base by gluing its bottom to a rigid support (a disk that is rigidly bolted to a shaker, such disk is technically called “fixture”); the connection is on the lateral surface of the shell, in order to increase the gluing surface, see Figure 2. A similar connection is carried out on the top; in this case the shell is connected to a disk made of aluminium alloy, such a disk is not externally constrained; therefore, it induces a rigid body motion to the top shell end.

The use of P.E.T. is due to reasons that are beyond the purpose of the present paper. Indeed, the same setup is used to perform experiments on dynamic instability, which gives rise to high amplitude of oscillation; in order to avoid plasticity for such high amplitudes the PET polymer is considered. This polymer showed a good linear behaviour, both from elastic and dissipation point of view, as proven by excellent curve fittings obtained from experimental data. Material characteristics are measured (E and ρ) or found in literature (ν).

The fixture is bolted to a high power shaker (LDS V806, 9000N peak force, 100g maximum acceleration, 300kg payload, 1-3000Hz band frequency); such shaker is used to excite the shell from the base or to provide a stiff support when the excitation is provided with different devices.

When the shell excitation is not furnished from the base, two kinds of excitation sources are applied: a micro shaker (TIRAVIB, 10N peak force, see Figure 3a) or a micro hammer.

As mentioned in the theoretical description, such case is much more complex than previous cases; the system exhibits both beam-like modes and shell-like modes (axisymmetric and asymmetric).

Experiments have been carried out by using different kind of excitation; indeed, the system characteristics makes difficult to excite all modes together. The first beam like mode is excited using a shaker connected to the top disk, see Figure 3a, this kind of excitation allows to transfer energy to the shell through the rigid body motion of the top disk; the energy path will excite only modes having a rigid body motion of the top-disk orthogonal to the shell axis, i.e. mainly beam modes. A second type of excitation is provided by exciting the shell from the base motion

(Figure 3b); it was observed experimentally that such kind of excitation pumped energy to the first axisymmetric mode and the second beam like mode; other modes were scarcely excited. The third kind of excitation was carried out by means of a micro-hammer; such kind of excitation allowed to furnish energy directly to shell modes having $n>1$. It is to note that the use of a micro hammer allows to furnish a small amount of energy to the system; therefore, all modes for which the motion of the top disk is present (n=0 or 1) are not excited, because the energy pumped in the system is not enough to induce a disk motion detectable from sensors (accelerometers). The combination of three types of excitation allowed to identify all modes within the frequency range of interest.

Mode		Natural frequencies [Hz]				
		Experimental frequency	Present theory		Finite elements	
k	*n*		Frequency	Error %	Frequency	Error%
first beam like mode *n*=1		95	96	1.1	93	2.1
1	0	314	322	2.5	314	0
second beam like mode *n*=1		438	432	2.5	424	3.2
1	6	791	797	0.8	782	1.1
1	7	816	802	1.7	802	1.7
1	5	890	888	0.2	885	0.6
1	8	950	926	2.5	918	3.4
1	9	1069	1016	5.0	1103	3.2

Table 4. Disk on the top, case C: comparison of natural frequencies: present theory vs. finite elements and experiments. Polynomials of degree 9 for the present theory.

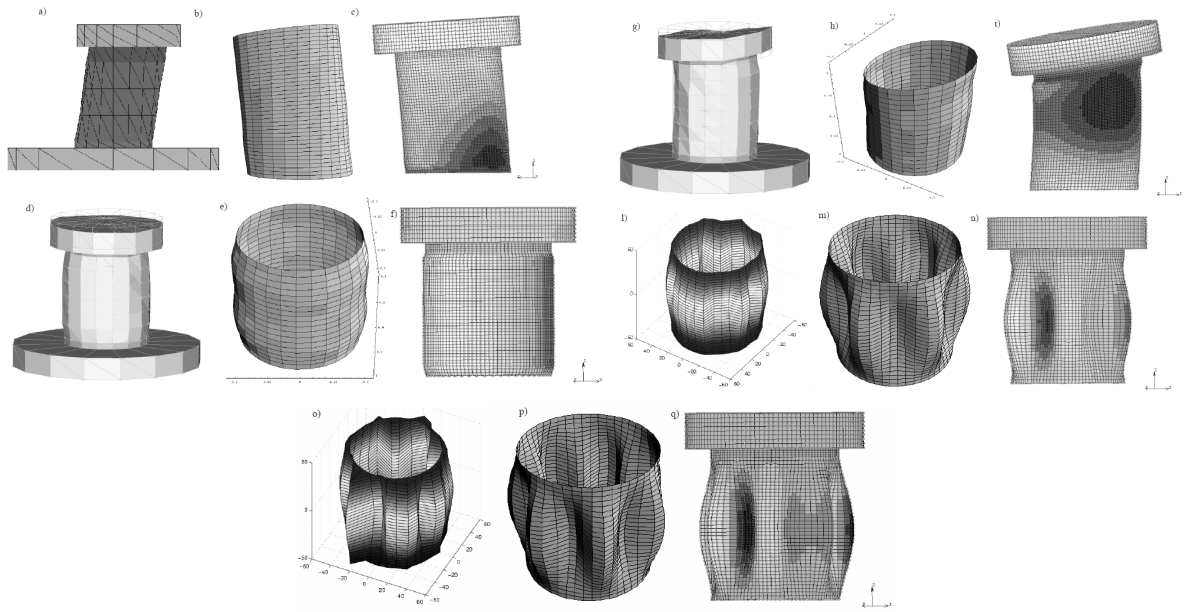

Figure 6. Mode shape comparisons: a), d), g), l) o) experiments; b) e) h) m) p) present theory; c) f) i) n) q) finite elements. a) b) c) first beam like mode n=1 (95Hz); d) e) f) mode (1,0) (314Hz); g) h) i) second beam-like mode n=1 (438Hz); l) m) n) mode (1,6) (791Hz); o) p) q) mode (1,7) (816Hz). Mode shape a) is reprinted from Ref. [19].

In Table 4 experimental, analytical and finite element results are presented: k means that the mode has k-1 nodal circumferences; n is the number of nodal diameters (beam modes can be considered n=1); FEM results are obtained by discretizing the shell similarly to the previous section, the top disk is discretized using brick elements in order to check possible disk structural vibration. All modes are identified experimentally by using curve fitting techniques, present in LMS CADA-X, that give: frequency, modal damping ratio, and modal shape. A 3D geometry of the system has been created before measurements, in order to associate each measurement to the corresponding point (and degree of freedom) on the geometry. The mode shape identification is of crucial importance in the case of shells; indeed, the high modal density makes difficult to compare experimental and teoretical/numerical modes using natural frequencies only; therefore, the visualization of modes is mandatory. Comparisons reported in Table 4 show that there is an excellent agreement among experiments, theory and finite elements. It is worthwhile to underline that finite element results have been obtained after a heavy computation both from time computing and memory usage points of view.

In Figure 6 mode shapes are reported both from experiments, theory and finite elements. The first mode (reprinted from Ref. [19]) is a beam-like mode; such kind of modes show doth displacement and rotation of the top-disk. The rotation is lost in the experiments because accelerometers are located radially in this first set of

measurements. In Ref. [19] beam modes were both experimentally and theoretically, using a simplified approach for solving Sanders-Koiter equations; such approach did not give accurate results for higher order modes. The second mode is axisymmetric, in this case the disk undergoes to a pure translation motion. In the theoretical description of the second mode, some longitudinal ripples are visible, which are due to the accuracy used in computations. Indeed, the sharp variation of curvature at the ends is an edge effect particularly evident for the first axisymmetric mode; this induces some convergence problems in the polynomial expansion. However, such shape inaccuracy does not affect the frequency estimation. A final note is needed for shell like modes (n>1): a micro hammer and a micro accelerometer have been used, the latter one is extremely light (0.25 10^{-3} kg); however, it induces a mass effect which causes an increasing of the radial deformation where the accelerometer is located.

Results and comparisons presented in this section show that the analytical approach developed in the present work is capable to predict, with good accuracy, linear vibrations of circular cylindrical shells having different and complex boundary conditions.

7. NONLINEAR ANALYSIS: NUMERICAL RESULTS AND COMPARISONS

Large amplitude of oscillations are analyzed for Case A shell; such geometry was deeply investigated in the past, see Refs. [14-17]. The shell is excited by means of a modal distributed force $q_r = f_{1,6}\sin(\eta)\cos(6\theta)\cos(\Omega t)$ (see also equation (7)) having amplitude equal to $f_{1,6} = 0.0012h^2\rho\omega_{1,6}^2$ and frequency close to the (k=1,n=6) mode frequency: $\Omega\cong\omega_{1,6}=2\pi\times553.3$ rad/s; the modal damping ratio considered in the calculations is 0.0005.

In the expansions (26) the following modes having k longitudinal half waves and n nodal diameters, identified by (k,m), are selected: longitudinal displacement field, (1,0), (3,0), (1,6); circumferential displacement field, (1,6), (1,12), (3,12); radial displacement field, (1,0), (3,0), (1,6). After selecting such modes, each expansion present in equations (16) is reduced to a three-terms expansion; the resulting dynamical system has 9 degrees of freedom.

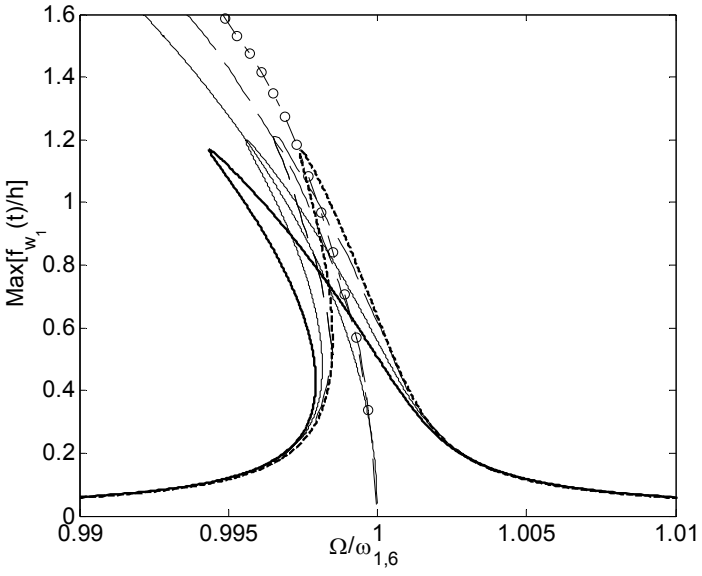

Figure 7. Nonlinear response. '▬ ▬'present theory; '–○–' Ref. [14]; '— —' Ref. [15]; '—' Ref. [16]; '▬' Ref. [17].

In Figure 7 the amplitude frequency curve is shown: this figure represents the maximum amplitude of vibration vs. the excitation frequency. Numerical results are obtained by means of the continuation software AUTO [18] that allows to find and follow periodic solutions of ordinary differential equations systems.

The response is slightly softening as confirmed by comparisons with Refs. [14-17]: the present model shows nonlinearity very close to Ref. [14], Refs.[15-17] predict larger nonlinear softening behaviour. It is to note that in Refs. [16,17] Donnell's nonlinear shallow shell theory is considered: this theory is less accurate than Sanders-Koiter theory, the static condensation of in-plane displacements and simplified kinematics reduce the accuracy; generally the Donnell's nonlinear shallow shell theory magnifies the softening behaviour.

It is worthwhile to stress that, in the past, several theoretical and numerical studies failed in predicting the correct nonlinear behaviour: often, spurious hardening behaviours were found. Recently, it was clarified that circular cylindrical shells generally show a softening behaviour [17]: only very short or very thick shells can have hardening behaviour. Therefore, the analysis presented is Figure 7 is an important benchmark for evaluating the accuracy of the method.

Note that the companion mode analysis has not been included in the model, because such deeper analysis is beyond the purposes of the present work.

8. CONCLUDING REMARKS

In this work both theoretical and experimental analyses have been carried out on shells vibration. Linear and nonlinear vibrations of circular cylindrical shells are analyzed by means of Sanders-Koiter theory. The proposed method is based on a mixed expansion including both harmonic functions and orthogonal polynomials. The approach is effective in respecting complex boundary conditions as confirmed by several comparisons with experiments and finite element methods. Such approach gives a general framework that allows to respect boundary conditions in a systematic way. Comparisons between theory and experiments are carried out both on natural frequencies and mode shapes.

The method has been tested in the case of large amplitude of vibration; also in this case the comparison with authoritative literature shows a good accuracy.

ACKNOWLEDGMENTS

The author thank Prof. Amabili for scientific discussions and suggestions; Mr. Boglione and Mr. Vergnano for experiments.

REFERENCES

[1] A.W. Leissa, *Vibration of Shells*, NASA SP-288. Washington, DC: Government Printing Office. Now available from The Acoustical Society of America, 1993.

[2] M. Amabili, M.P. Païdoussis, Review of studies on geometrically nonlinear vibrations and dynamics of circular cylindrical shells and panels, with and without fluid-structure interaction. *Applied Mechanics Reviews,* **56** (2003) 349-381.

[3] K.M. Liew, M.K. Lim, C.W. Lim, D.B. Li, Y.R. Zhang, Effects of initial twist and thickness variation on the vibration behaviour of shallow conical shells, *Journal of Sound and Vibration*, **180**(2) (1995) 271-296.

[4] A. Bhaskar, P. C. Dumir, Non-linear vibration of orthotropic thin rectangular plates on elastic foundations, *Journal of Sound and Vibration*, **125**(1) (1988) 1-11.

[5] K.M. Liew, T.Y. Ng, X. Zhao, Free vibration analysis of conical shells via the element-free kp-Ritz method, *Journal of Sound and Vibration*, **281 (**2005) 627-645.

[6] X. Zhao, T.Y. Ng, K.M. Liew, Free vibration of two-side simply-supported laminated cylindrical panels via the mesh-free kp-Ritz method, *International Journal of Mechanical Science*, **46 (**2004) 123-142.

[7] D. Zhou, Y.K. Cheung, S.H. Lo, F.T.K. Au, 3D vibration analysis of solid and hollow circular cylinders via Chebyshev–Ritz method, *Computer Methods Applied Mechanics Engineering*, **192 (**2003) 1575–1589.

[8] K. P. Soldatos, A. Messina, Vibration Studies of cross-ply laminated shear deformable circular cylinders on the basis of orthogonal polynomials, *Journal of Sound and Vibration*, **218**(2) (1998) 219-243.

[9] A. H. Nayfeh, H. N. Arafat, Nonlinear Dynamics of Closed Spherical Shells, *Proceedings of DETC2005 ASME 2005 Int. Design Eng. Technical Conferences & Computers and Information in Engineering Conference, September 2005, Long Beach, California USA*, paper N. DETC2005-85409.

[10] V. A. Trotsenko and Yu. V. Trotsenko, Methods for calculation of free vibrations of a cylindrical shell with attached rigid body. *Nonlinear Oscillations*, **7**(2) (2004) 262-284.

[11] Y.V. Trotsenko, Frequencies and modes of vibration of a cylindrical shell with attached rigid body, *Journal of Sound and Vibration*, **292** (2006) 535-551.

[12] N. Yamaki, *Elastic Stability of Circular Cylindrical Shells*, North-Holland, Amsterdam, 1984.

[13] M. A. Snyder, *Chebyshev methods in numerical approximation*, Prentice-Hall, London, 1966.

[14] M. Ganapathi and T. K. Varadan, Large Amplitude Vibrations of Circular Cylindrical Shells, *Journal of Sound and Vibration*, **192**(1) (1996) 1-14.

[15] J. C. Chen and C. D. Babcock, Nonlinear Vibration of Cylindrical Shells, *AIAA Journal*, **13**(7) (1975) 868-876.

[16] M. Amabili, F. Pellicano and A. F. Vakakis, Nonlinear Vibrations and Multiple Resonances of Fluid Filled Circular Shells; Part 1: Equation of Motion and Numerical Results, *Journal of Vibration and Acoustics,* **122**(1) (2000) 346-354.

[17] F. Pellicano, M. Amabili and M.P. Païdoussis, Effect of the Geometry on the Non-Linear Vibration of Circular Cylindrical Shells, *International Journal of Nonlinear Mechanics*, **37 (**2002) 1181-1198.

[18] E.J. Doedel, A.R. Champneys, T.F. Fairgrieve, Y.A. Kuznetsov, B. Sandstede, X. Wang, *AUTO 97: Continuation and Bifurcation Software for Ordinary Differential Equations (with HomCont)*. Concordia University, Montreal, Canada, 1998.

[19] F. Pellicano and K. V. Avramov, Dynamic Instability of a Seismically Excited Circular Cylindrical Shell with Attached Disk, *Communications in Nonlinear Science and Numerical Simulation*, 2004 (in press)